JOURNAL OF GEOPHYSICAL RESEARCH, VOL. 103, NO. A10, PAGES 23,551–23,563, OCTOBER 1, 1998

Modeling of twisted/warped magnetospheric configurations using the general deformation method

N. A. Tsyganenko

Raytheon STX Corporation, Laboratory for Extraterrestrial Physics, NASA Goddard Space Flight Center
Greenbelt, Maryland

Abstract. A new method is developed for modeling the effects of the planetary dipole tilt and of the interplanetary magnetic field (IMF) related twisting of the cross-tail current sheet. The method extends the field deformation technique of *Stern* [1987] and makes it possible to easily represent a wide variety of warped magnetospheric configurations, starting from simple models with an axially symmetric magnetopause and a planar tail current sheet. The proposed transformations do not violate the condition $\nabla \cdot \mathbf{B} = 0$ and allow one to retain a desired distribution of the normal component of the total field at the magnetospheric boundary. Furthermore, the method makes it possible to add flexibility to the model magnetopause, so that the effects of the dipole tilt and of the IMF upon its shape can be reproduced. In particular, the transformation with a radially dependent rotation of the X and Z axes, while providing the desired tilt-related bending of the cross-tail current sheet, can also deform the magnetopause and reproduce its tilt-related asymmetry, indicated by observations and reported here for the first time. The deformation technique also allows algorithms that are more compact and faster than the currently used ones. Because of the general nature of the proposed approach it should be possible to extend it to the modeling of other (e.g., Jovian) planetary magnetospheres.

1. Introduction

Analytical data-based models of the geomagnetic field are widely accepted as a tool for reproducing the global configuration of the magnetosphere under different solar wind conditions. To replicate a wide variety of possible field geometries, one has to represent the contributions to the field from the principal magnetospheric currents in flexible mathematical formats. Such flexibility can be provided in principle by increasing the number of terms in the expansions for the magnetic field components. However, making the models more and more complex conflicts with the requirement that they should also be mathematically compact to ensure their computational efficiency. Reconciling these opposing demands is quite a challenging task, since the shapes of the cross-tail current sheet and of the magnetopause are affected by the tilt of the planetary dipole and by the interplanetary magnetic field, which breaks down the symmetry expected with an untilted dipole and unmagnetized solar wind. As a result one is faced with the problem of representing the fields from warped and twisted current sheets, shielded within an asymmetric magnetospheric boundary.

Previous efforts to build analytical magnetospheric field models were only partially successful in solving these problems. Thus *Voigt* [1981] proposed a simple version of the stretch transformation, which allowed him to reproduce the observed tilt-related warping of the tail current sheet in the Y–Z plane. *Tsyganenko* [1989, 1995] and *Tsyganenko and Peredo* [1994] suggested a simple modification of the Z coordinate in the expansion for the vector potential of the tail current sheet, which made it possible to shift the maximum of the electric current density away from the equatorial plane and thus represent the warping of the sheet in two dimensions.

All the above models assumed an axially symmetric magnetopause with a fixed shape and position, ignoring its possible dependence on the dipole tilt. As will be shown in section 3.1, that assumption is generally not true. Besides that, no dependence of the tail current position on the IMF B_y was assumed in previous models, even though the related "twisting" effect was predicted [*Russell,* 1972] and was found to be quite significant even at relatively close geocentric distances [*Sibeck et al.,* 1985, 1986a; *Tsyganenko,* 1990; *Tsyganenko et al.,* 1998].

Another difficulty in modeling the warped/twisted cross-tail current sheet is the need to keep the total field fully shielded within the model magnetopause (or, in a more general case, to keep under control the normal component B_n on the magnetopause) for any shape of the sheet. In that respect, changing the value of the dipole tilt angle would require the shielding field to be recalculated over and over again, resulting in unacceptably slow and cumbersome codes. *Tsyganenko* [1995, 1996] handled that problem by adding a group of tilt-dependent terms in the expansions for the shielding field. However, the model field is a superposition of several terms or "modules," representing contributions from the dipole, cross-tail current, ring current, and region 1/2 Birkeland currents. The tail field itself is given by two or three submodules with different variation scale lengths in the X

Paper number 98JA02292.
0148-0227/98/98JA-02292$09.00

direction. Each of those modules has its own variation and amplitude and hence requires a separate group of terms for the shielding field. For that reason, taking into account the dipole tilt by further extending the shielding field expansions comes at a significant price in terms of the computation speed.

All the above reasons motivated us to search for a simple and general procedure for flexibly modifying model magnetic fields. In a recent work, *Tsyganenko* [1997] proposed a simple model of the magnetic field from the substorm current wedge, which took into account the warping of the current system in response to the geodipole tilt. In that model a radially dependent rotation of coordinate axes around the Y_{GSM} direction was introduced, and it also required the components of the vector potential of the deformed field to be known in explicit form.

The goal of the present paper is to describe a universal procedure for warping and twisting the tail current sheet, a procedure that also allows one to control the shape of the magnetopause, making it consistent with data and with results of MHD simulations. All the deformations developed in this work are derived from a general method, based on Euler potentials and first described by *Stern* [1987].

As will be discussed below in more detail, the method does not require the Euler potentials to be known: it is only necessary and sufficient to specify the components of the undeformed magnetic field and to devise an appropriate transformation of the coordinates. Another important feature of the method is that the desired final configuration of the magnetic field can be obtained in a stepwise manner by superposing consecutive "partial" deformations, so that each of them is carried out in its own coordinate system, best suited for that specific transformation from the viewpoint of its symmetry properties.

On the basis of the above considerations the paper is organized as follows. Section 2 describes the general deformation method, without going into the details of its particular applications. Section 3 deals with the partial deformation of the magnetosphere due to the tilt of the Earth's dipole, replicating the observed bending of the magnetotail and its departure from the GSM equatorial plane, when viewed in the X–Z projection. It also presents observational evidence for a north-south asymmetry of the magnetopause, associated with the dipole tilt, and shows how the deformation method accommodates that effect. Section 4 presents a group of partial transformations, which yield (1) the tilt-related warping of the cross-tail current in the GSM Y–Z plane, (2) variable broadening of the current sheet toward its flanks, and (3) the effect of the current sheet twisting in response to the IMF B_y. Section 5 summarizes the results of the present study.

2. General Method

The purpose of this section is to outline a general method of deforming magnetic fields, based on Euler potentials, and to extend the Cartesian transformation, proposed by *Stern* [1987, equation (45)], to arbitrary orthogonal coordinates.

Consider a magnetic field $\mathbf{B} = \mathbf{B}(f, g, h)$, where the coordinates (f, g, h) refer to any orthogonal system (e.g., Cartesian, cylindrical, or spherical.) Suppose that the field is represented by a pair of Euler potentials, α and β:

$$\mathbf{B}(f, g, h) = \nabla\alpha(f, g, h) \times \nabla\beta(f, g, h) \tag{1}$$

The gradients on the right-hand side of (1) can be explicitly written [e.g., *Stern*, 1987, equation (12)] as

$$\nabla\alpha = \frac{1}{H_f}\frac{\partial\alpha}{\partial f}\mathbf{e}_f + \frac{1}{H_g}\frac{\partial\alpha}{\partial g}\mathbf{e}_g + \frac{1}{H_h}\frac{\partial\alpha}{\partial h}\mathbf{e}_h$$
$$\nabla\beta = \frac{1}{H_f}\frac{\partial\beta}{\partial f}\mathbf{e}_f + \frac{1}{H_g}\frac{\partial\beta}{\partial g}\mathbf{e}_g + \frac{1}{H_h}\frac{\partial\beta}{\partial h}\mathbf{e}_h \tag{2}$$

where $\{\mathbf{e}_f, \mathbf{e}_g, \mathbf{e}_h\}$ and $\{H_f, H_g, H_h\}$ are unit vectors and scale factors, respectively, corresponding to the coordinates $\{f, g, h\}$.

From (1)–(2) the components of the undistorted field (1) read as

$$B_f = \frac{1}{H_g H_h}\left(\frac{\partial\alpha}{\partial g}\frac{\partial\beta}{\partial h} - \frac{\partial\beta}{\partial g}\frac{\partial\alpha}{\partial h}\right)$$
$$B_g = \frac{1}{H_f H_h}\left(\frac{\partial\alpha}{\partial h}\frac{\partial\beta}{\partial f} - \frac{\partial\beta}{\partial h}\frac{\partial\alpha}{\partial f}\right) \tag{3}$$
$$B_h = \frac{1}{H_f H_g}\left(\frac{\partial\alpha}{\partial f}\frac{\partial\beta}{\partial g} - \frac{\partial\beta}{\partial f}\frac{\partial\alpha}{\partial g}\right)$$

Let us define a deformation of the original field by replacing the "old" coordinates (f, g, h) in the Euler potentials in (1) with distorted "new" ones (ξ, η, ζ), respectively, so that the deformed magnetic field

$$\mathbf{B}'(f, g, h) = \nabla\alpha(\xi, \eta, \zeta) \times \nabla\beta(\xi, \eta, \zeta) \tag{4}$$

where the new coordinates $\xi = \xi(f, g, h)$, $\eta = \eta(f, g, h)$, and $\zeta = \zeta(f, g, h)$ are known functions of the old ones.

The components of the "new" (deformed) field (4) in the "old" orthonormal basis $\{\mathbf{e}_f, \mathbf{e}_g, \mathbf{e}_h\}$ can be obtained by expanding all the partial derivatives in (3) according to the chain differentiation rule, e.g.,

$$\frac{\partial\alpha}{\partial f} = \frac{\partial\alpha}{\partial\xi}\frac{\partial\xi}{\partial f} + \frac{\partial\alpha}{\partial\eta}\frac{\partial\eta}{\partial f} + \frac{\partial\alpha}{\partial\zeta}\frac{\partial\zeta}{\partial f}$$

and so on. For each of the three components of $\mathbf{B}'$ this expansion results in 18 terms, of which six cancel each other and the remaining 12 can be regrouped, so that the modified field assumes a compact form

$$\mathbf{B}' = \hat{\mathbf{T}}\mathbf{B}^* \tag{5}$$

where the asterisk indicates that the field $\mathbf{B}^*$ is obtained by replacing, in each component B_f, B_g, and B_h of the undeformed field $\mathbf{B}$, the original coordinates $\{f, g, h\}$ with $\{\xi(f, g, h), \eta(f, g, h), \zeta(f, g, h)\}$, but keeping the same unit vectors as in (2). The elements of the matrix $\hat{\mathbf{T}}$ read as follows

$$T_{ff} = \frac{H_g^* H_h^*}{H_g H_h}\left(\frac{\partial\eta}{\partial g}\frac{\partial\zeta}{\partial h} - \frac{\partial\eta}{\partial h}\frac{\partial\zeta}{\partial g}\right)$$
$$T_{fg} = \frac{H_f^* H_h^*}{H_g H_h}\left(\frac{\partial\xi}{\partial h}\frac{\partial\zeta}{\partial g} - \frac{\partial\xi}{\partial g}\frac{\partial\zeta}{\partial h}\right)$$
$$T_{fh} = \frac{H_f^* H_g^*}{H_g H_h}\left(\frac{\partial\xi}{\partial g}\frac{\partial\eta}{\partial h} - \frac{\partial\xi}{\partial h}\frac{\partial\eta}{\partial g}\right)$$

$$
\begin{aligned}
T_{gf} &= \frac{H_g^* H_h^*}{H_f H_h}\left(\frac{\partial\eta}{\partial h}\frac{\partial\zeta}{\partial f} - \frac{\partial\eta}{\partial f}\frac{\partial\zeta}{\partial h}\right)\\
T_{gg} &= \frac{H_f^* H_h^*}{H_f H_h}\left(\frac{\partial\xi}{\partial f}\frac{\partial\zeta}{\partial h} - \frac{\partial\xi}{\partial h}\frac{\partial\zeta}{\partial f}\right)\\
T_{gh} &= \frac{H_f^* H_g^*}{H_f H_h}\left(\frac{\partial\xi}{\partial h}\frac{\partial\eta}{\partial f} - \frac{\partial\xi}{\partial f}\frac{\partial\eta}{\partial h}\right)\\
T_{hf} &= \frac{H_g^* H_h^*}{H_f H_g}\left(\frac{\partial\eta}{\partial f}\frac{\partial\zeta}{\partial g} - \frac{\partial\eta}{\partial g}\frac{\partial\zeta}{\partial f}\right)\\
T_{hg} &= \frac{H_f^* H_h^*}{H_f H_g}\left(\frac{\partial\xi}{\partial g}\frac{\partial\zeta}{\partial f} - \frac{\partial\xi}{\partial f}\frac{\partial\zeta}{\partial g}\right)\\
T_{hh} &= \frac{H_f^* H_g^*}{H_f H_g}\left(\frac{\partial\xi}{\partial f}\frac{\partial\eta}{\partial g} - \frac{\partial\xi}{\partial g}\frac{\partial\eta}{\partial f}\right)
\end{aligned}
\qquad (6)
$$

where, again, the asterisks by the scaling factors indicate that they should be calculated at the mapped location $\{\xi, \eta, \zeta\}$, instead of the original one $\{f, g, h\}$. As was the case for the cartesian transformation of *Stern* [1987], the general deformation (5)–(6) still retains a very important advantage of the former one: the components of the deformed field are linear combinations of those pertaining to the undeformed field, in which the variables (f, g, h) are replaced by (ξ, η, ζ), and hence we do not need to know the Euler potentials. It is also worth noting that, by construction, the deformed field remains divergence-free.

In the following sections, several particular implementations of the general procedure (5)–(6) will be developed, aimed at reproducing the large-scale distortion of the magnetosphere due to the effects of the IMF and of the dipole tilt angle.

3. Deformations in the X–Z Plane Related to the Dipole Tilt

This section concentrates on a deformation, yielding the observed gradual deflection of the magnetotail away from the equatorial plane of the tilted planetary dipole. The principal idea behind the choice of an appropriate coordinate transformation is that at close geocentric distance the magnetic configuration is rigidly tied to the geodipole and sways back and forth around the Y_{GSM} axis, while at larger distances it forms the magnetospheric tail, which gradually aligns itself parallel to the solar wind flow, inclined at an angle Ψ with respect to the dipolar equatorial plane. The coordinate transformation should therefore provide a gradual transition between these two regimes at geocentric distances of $\sim 10\,R_E$, where the dipole field magnitude becomes comparable with the field in the near-tail lobes.

A simple way to quantitatively represent this effect is to start from a magnetospheric model with an untilted dipole (and hence with a planar tail current sheet) and, following the procedure (5)–(6), introduce a deformation of Cartesian coordinates in which any point (X, Y, Z) is mapped to "quasi-solar magnetic" coordinates (X^*, Y^*, Z^*) with a radially-dependent tilt angle Ψ^* [*Tsyganenko and Stern,* 1996; *Tsyganenko,* 1997], so that

$$
\begin{aligned}
X^* &= X\cos\Psi^*(r) - Z\sin\Psi^*(r)\\
Y^* &= Y\\
Z^* &= X\sin\Psi^*(r) + Z\cos\Psi^*(r)
\end{aligned}
\qquad (7)
$$

In the limit $r \to 0$ the angle Ψ^* should become equal to the geodipole tilt angle Ψ, so that near Earth the coordinates (X^*, Y^*, Z^*) tend to the standard solar magnetic ones, while at large distances they asymptotically tend to the solar magnetospheric coordinates. An additional requirement should also be met at large distances, namely,

$$
r\sin\Psi^* \approx R_H\sin\Psi \qquad \text{for} \quad r \gg R_H\,, \qquad (8)
$$

where R_H is the "hinging distance," defining the amplitude of the tilt-induced oscillation of the tail current sheet around its average position.

Equation (8) implies that the hinging distance R_H does not depend on r and hence the tilt-related motion of the current sheet does not disappear in the deep tail. This assumption is supported by results of a recent statistical study of the cross-tail current, based on an extensive set of Geotail data [*Tsyganenko et al.,* 1998].

The above constraints upon the radial behavior of Ψ^* suggest defining it by

$$
\sin\Psi^* = Q(r)\sin\Psi\,, \qquad (9)
$$

where $Q(0) = 1$ and $Q(r) \approx R_H/r$ for $r \to \infty$. A very simple choice for the function $Q(r)$, satisfying both conditions, is

$$
Q(r) = \left[1 + \left(\frac{r}{R_H}\right)^{\epsilon}\right]^{-\frac{1}{\epsilon}}\,. \qquad (10)
$$

The function Q in (10) still contains a free parameter ϵ, whose value can be specified on the basis of the following simple considerations.

In the region where $\mathbf{B}$ is quasi-dipolar (which approximately holds for $r \le R_H$) the tilt-related distortion of the initial north-south symmetry of the field can be attributed, in a crude approximation, to a nonzero contribution from an external field in the direction perpendicular to the dipole axis and proportional to $\sin\Psi$. In comparison with the dipole field, which rapidly varies with radial distance, the external field is much smoother and hence can be approximated in the vicinity of the dipole by a uniform perturbation vector $\Delta\mathbf{B}$, which in the case $\Psi \neq 0$ has a component along the solar magnetic X axis. Using these assumptions, one can easily show that the resultant deflection of distorted dipolar field lines away from unperturbed ones grows with geocentric distance as $\sim r^4$, at both high and low dipole latitudes.

On the other hand, the tilt-induced deflection of the dipole field lines approximately equals $r(\Psi^* - \Psi)$, and hence $\Psi^* - \Psi \sim r^3$. Combined with (9) and (10), this immediately yields $\epsilon = 3$, and hence (9) takes the form

$$
\sin\Psi^* = \frac{R_H\sin\Psi}{(R_H^3 + r^3)^{1/3}} \qquad (11)
$$

Figure 1 shows the result of applying the radially-dependent tilt deformation (7) with Ψ^* defined by (11), $R_H = 7\,R_E$, and $\Psi = 30°$, to the initially untilted field, given by a data-based model [*Tsyganenko,* 1996]. As can be seen from the plots, the deformation method provides at least a "visually reasonable" configuration. However, two important comments should be made, as discussed in the following sections 3.1 and 3.2.

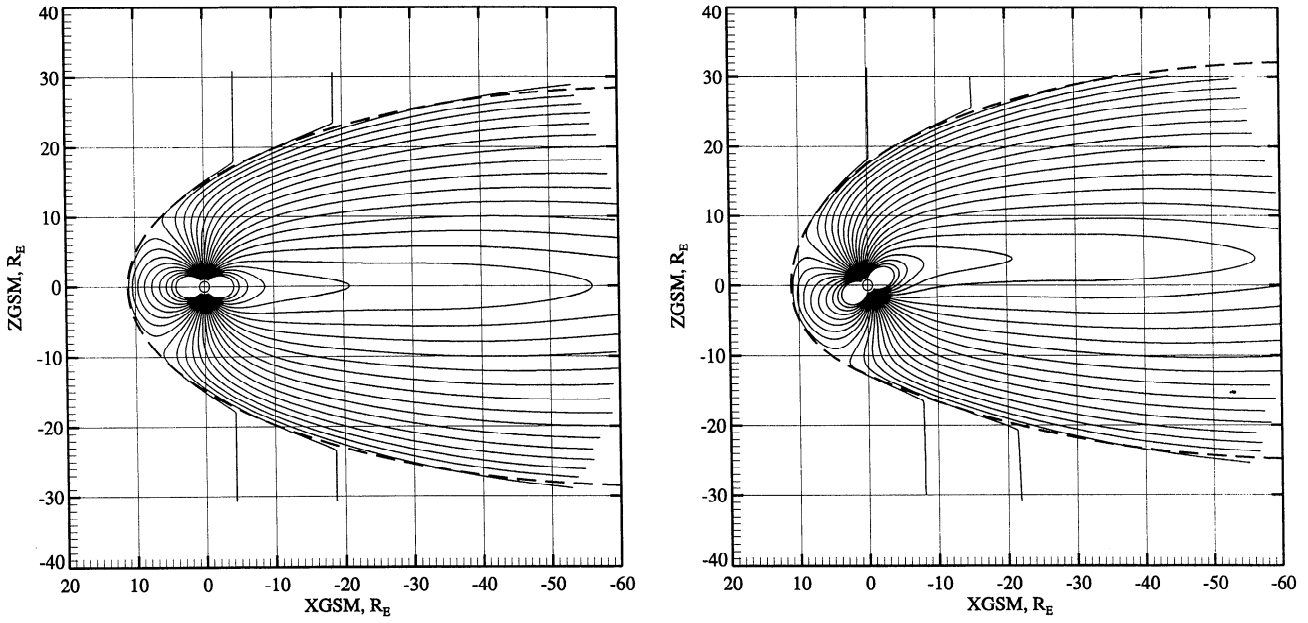

Figure 1. Illustration of the effect of the radially dependent rotation, showing the tilt-related deformation of the entire model magnetosphere. (left) The untilted model magnetosphere; (right) the same field configuration modified by the transformation (6)–(10) with $\Psi = 30°$, $R_H = 7\,R_E$. The field lines are plotted with 2° intervals of the foot point latitude, starting from 60°. Note the lack of tilt angle dependence of the polar cusp field lines mapping into the vicinity of the dayside neutral points.

3.1. Tilt-Related Deformation of the Magnetopause

The deformation (7) affects not only the shape of the tail current sheet but the entire magnetosphere, including the magnetopause, which shifts along the Z axis in the same direction and with the same amplitude as the cross-tail current sheet, as can be seen in Figure 1. To what extent does this purely mathematical effect reflect an actual tilt-related deformation of the magnetopause ?

An indirect piece of evidence in favor of the existence of a tilt-related motion of the magnetopause in the tail was given by *Tsyganenko et al.* [1998], who found from Geotail data that even in the far tail ($X \sim -100\,R_E$) the cross-tail current sheet oscillates in the Z direction with the same amplitude as that in the near tail. At the same time the warping of the sheet's cross section in the Y–Z plane gradually disappears with growing tailward distance. On the basis of the requirement of pressure balance between tail lobes with equal magnetic fluxes, one has to conclude that the northern and southern lobes should also have equal cross-sectional areas. The only way to satisfy this requirement is to admit that the tail magnetopause moves in the Z direction in concert with the tilt-induced motion of the central cross-tail current sheet.

To verify that conjecture, we made a statistical study of the position of the tailward magnetopause, based on direct observations of the boundary in the range of distances $-40 \le X \le -20\,R_E$. The data were taken from the set of *Sibeck et al.* [1991] and divided into five bins of the dipole tilt angle: $-35° \le \Psi \le -20°$, $-20° \le \Psi \le -10°$, $-10° \le \Psi \le 10°$, $10° \le \Psi \le 20°$, and $20° \le \Psi \le 35°$. For each data subset a best fit ellipse was found, representing the average shape of the magnetopause in the tail cross section. Figure 2 shows the result of the fitting for three bins of Ψ, corresponding to large negative, small, and large positive tilt angles. A distinct shift of the boun- dary in the positive Z direction with increasing tilt angle can be clearly seen in the plots: for the three intervals of Ψ, specified above, the centers of the best fit ellipses were found at $Z = -3.3 \pm 0.4\,R_E$, $Z = -0.1 \pm 0.4\,R_E$, and $Z = 2.3 \pm 1.3\,R_E$, respectively. In fitting the ellipses to the crossing data their size, position, and eccentricity were considered as free parameters, while the scatter in the observed positions of the boundary with respect to the elliptical cross sections was assumed to obey the normal distribution law.

On the basis of those assumptions we calculated uncertainties of each of the variable parameters. Centers of the best fit ellipses are shown in each panel by a rectangle with dimensions equal to the estimated uncertainties of the center's position along Y and Z axes. In the cases of strongly negative and relatively small tilt angles (left and middle panel) the centers were found with a greater confidence, owing to larger number of data points, so that the typical uncertainty in both dimensions is about $0.4\,R_E$. In the right panel, corresponding to strongly positive tilt angles, the number of data points is much smaller, and the uncertainty rises up to $1.3\,R_E$; however, as can be seen from the plot, the upward shift still remains siginificant. The eccentricity of the ellipses is relatively small in the left and middle panels, while in the right panel the best fit boundary is more elongated in the Y direction. However, because of the lack of data the uncertainty of the eccentricity is much higher in this case (~77%), so that the obtained variation of the magnetopause shape is, most probably, insignificant. Table 1 displays the parameters of ellipses, corresponding to all five bins of Ψ, including two

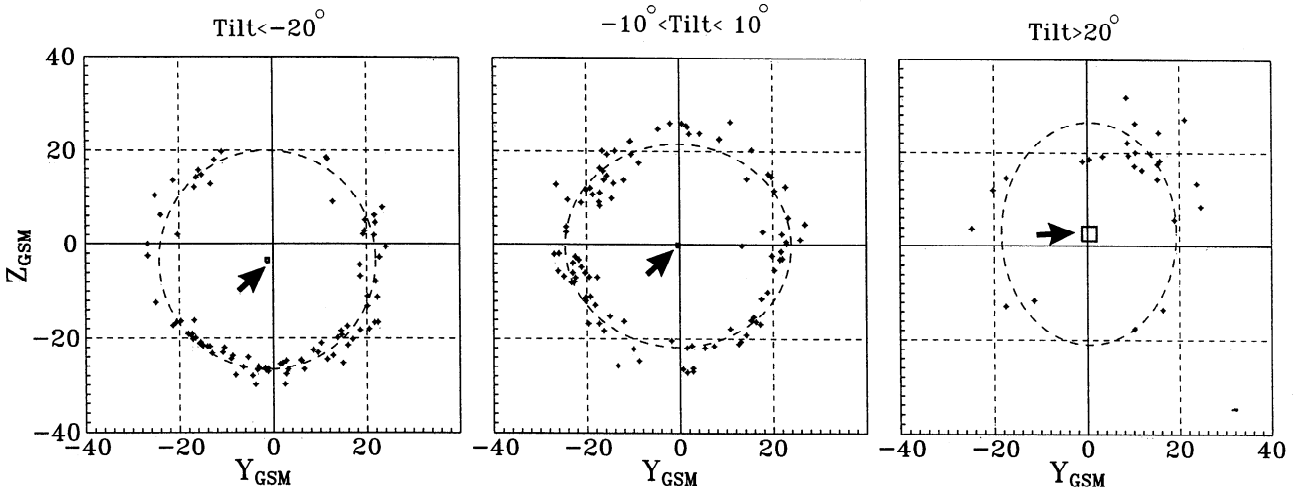

Figure 2. Effect of the Earth's dipole tilt upon the position of the magnetotail boundary along the Z axis in the distance range $-40 < X < -20\,R_E$. The observed crossings of the magnetopause [*Sibeck et al.*, 1991], binned into three intervals of the dipole tilt, are shown by dots. The elliptical best fit positions of the boundary cross section are shown by dashed lines in each panel. The rectangles, indicated by arrows, correspond to the calculated location of the center of the ellipses, approximating the average shape of the boundary. The size of the rectangles indicates the uncertainty of the center's position. Note a clear dependence of the boundary position on the dipole tilt angle.

intermediate intervals, not shown in Figure 2. Note that, contrary to what one would expect, the shift for the interval $10° \le \Psi < 20°$ was found to be negative. However, because there were fewer data points for positive tilt angles, the corresponding uncertainty of ΔZ is significantly larger in that case, so that the obtained anomalous negative value of the shift is unlikely to be real.

To specify more accurately the location of the magnetopause as a function of the dipole tilt, another study was done, based on the entire set of crossing data for all available tilt angles. In this approach the shift of the center of the best fit circle from the GSM equatorial plane was represented as a continuous function of the tilt angle: $R_H^{(m)} \sin\Psi$, i.e., in the same way as the position of the tail current sheet in first simple "hinging" models [e.g., *Murayama*, 1966]. The corresponding "magnetopause hinging distance" $R_H^{(m)}$ was determined by using a least squares fitting, based on all boundary crossings. It was found equal to $R_H^{(m)} = 5.66\,R_E$, somewhat less than a typical $R_H \sim 8\,R_E$ for the central tail current sheet, a result that appears quite reasonable. Indeed, the magnetopause is located, in general, at larger geocentric distances than is the inner edge of the tail current, and it is more directly exposed to the solar wind, which makes its shape less sensitive to the dipole tilt.

Using the data from high-latitude, high-apogee spacecraft, such as HEOS and Hawkeye 1, one can in principle deduce tilt-related effects on the shape of the magnetopause for other intervals of X, which would make it possible to devise more elaborate deformations. The simplest way of adding more flexibility to the deformation (7)–(11) is to make the hinging distance R_H a function of position. For example, we can take R_H in the form

$$R_H = R_{H0} + R_{H1}\frac{Z}{r}\sin\Psi + R_{H2}\frac{Z^2}{r^2} \qquad (12)$$

Assuming the coefficient $R_{H2} < 0$ yields the desired weaker response of the tailward magnetopause to the dipole tilt, as compared with that of the central current sheet. The second term in the right-hand side of (12) provides a north-south asymmetry of the deformation: assuming $R_{H1} > 0$

Table 1. Parameters of Ellipses Approximating the Shape of the Tail Boundary by $(Y-\Delta Y)^2+(1-\epsilon)(Z-\Delta Z)^2-R^2=0$, for Five Consecutive Bins of the Earth's Dipole Tilt Angle

	$-35° < \Psi < -20°$	$-20° < \Psi < -10°$	$-10° < \Psi < 10°$	$10° < \Psi < 20°$	$20° < \Psi < 35°$
N	85	75	101	36	26
σ	1.87	2.85	2.59	3.18	3.65
R	23.3±0.4	22.1±0.7	21.7±0.4	20.5±0.8	23.7±1.9
ΔY	-1.2 ± 0.3	-1.8 ± 0.5	-0.4 ± 0.4	1.0 ± 0.7	0.7 ± 1.6
ΔZ	-3.3 ± 0.4	-1.0 ± 0.5	-0.1 ± 0.4	-0.6 ± 1.5	2.3 ± 1.4
ϵ	0.0 ± 0.06	0.16 ± 0.08	0.20 ± 0.05	0.46 ± 0.08	-0.5 ± 0.4

The first two rows display the numbers of data points in each bin, N, and the residual rms deviation, σ, of the observed crossings from the best fit elliptical cross section. The results correspond to $-40\,R_E < X_{GSM} < -20\,R_E$.

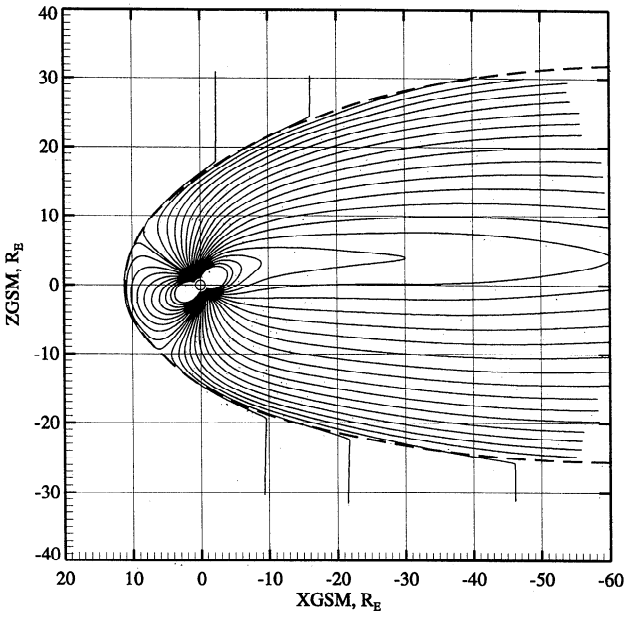

Figure 3. Same as Figure 1 (right) but obtained with the spatially dependent hinging distance R_H, given by (11) with $R_{H0} = 8$, $R_{H1} = 2$, $R_{H2} = -6$, and $\Psi = 30°$. Note a decrease in the asymmetry of the model magnetopause in comparison with that for the simpler deformation in Figure 1.

leads to a smaller deformation of the southern (northern) magnetopause for $\Psi > 0$ ($\Psi < 0$). Such an asymmetry was reported by *Eastman et al.* [1997] on the basis of a detailed study of high-latitude magnetopause crossings by Hawkeye 1. Figure 3 shows a tilted magnetospheric configuration, similar to that in Figure 1 but obtained with a variable hinging distance, given by (12) with $R_{H0} = 8$, $R_{H1} = 2$, $R_{H2} = -6$, and $\Psi = 30°$. With this choice of parameters the hinging distance peaks at low latitudes, so that the amplitude of the tilt-related oscillations is maximal at the location of the plasma sheet but becomes significantly smaller near the magnetopause, in agreement with the smaller value of $R_H^{(m)} = 5.66$, obtained for the magnetopause at $X \sim -30\, R_E$ (Figure 2).

3.2. Tilt Deformation and the Position of Model Polar Cusps

In this section we discuss another subtle problem inherent in the deformation technique, which concerns the magnetic field mapping between the ionosphere and magnetosphere. The problem originates in an intrinsic property of the deformation method, its conservation of the topology of the magnetic lines. More specifically, it means that for any continuous transformation of the old coordinates $\{f, g, h\}$ into the new ones $\{\xi, \eta, \zeta\}$, any individual field line will undergo a limited deformation, provided the Euler potentials are continuous and well-behaved functions of position.

With regard to the transformation (7), the topology conservation means that any individual line is subject to a limited amount of distortion, proportional to the tilt angle of the planetary dipole. In particular, the field lines passing through the null points of the magnetic field on the dayside magnetopause will change their shape with Ψ, but since we required $\Psi^* \approx \Psi$ at low altitudes, the conservation of the Euler potentials along the lines will result in the independence of their foot point magnetic latitude on Ψ. In terms of the magnetospheric geometry the above property means that the deformed model polar cusps will map to the same latitude in the ionosphere for all dipole tilt angles, as can be verified by a closer inspection of Figure 1. This conclusion disagrees both with observations and with data-based models: according to *Newell and Meng* [1989], the observed latitudinal shift of the polar cusps due to the dipole tilt reaches $3° - 4°$ for the maximal tilt angle of $\Psi = 35°$, which is close to the values given by models [*Tsyganenko,* 1990].

Apparently, there is no simple way to circumvent that difficulty, as long as a single deformation of the total field is to represent all tilt-associated effects. A compromise solution is to apply the deformation techniqc to all external sources while retaining a tilt-dependent scalar potential for shielding the planetary dipole field, taking into account the tilt-related variation of the magnetopause shape. Shielding the dipole by a potential field does reproduce most of the tilt-related shift of the polar cusp foot points [e.g., *Stern,* 1985]. More details on the derivation of the shielding field for the Earth's dipole within a tilt-dependent magnetopause are given in the appendix.

4. Transformations Affecting the Magnetospheric Structure in the Tail's Cross Section

This section describes specific transformations representing the effects of the geodipole tilt and of the azimuthal component of the IMF upon the shape of the Y–Z cross sections of the magnetotail current sheet. As was already found in early observations [e.g., *Russell and Brody,* 1967; *Fairfield,* 1980], seasonal and diurnal oscillations of the Earth's dipole tilt angle result in a periodic warping of the cross-tail current sheet. That effect was extensively studied and modeled in many later works, including our most recent effort [*Tsyganenko et al.,* 1998, and references therein], which covered the largest range of tailward distances and revealed the dependence of the cross-tail current deformation on position along the Sun-Earth line.

In addition to the above, the magnetospheric tail is also twisted by the IMF, as was first conjectured by *Russell* [1972] and theoretically studied by *Cowley* [1981]. The first observational evidence for that effect came from ISEE 3 data taken in the deep tail [*Sibeck et al.,* 1985, 1986a]. *Tsyganenko* [1990] found clear signatures of such twisting from a statistical analysis of data taken at closer distances within $X \sim -65\, R_E$. In the most recent work, based on Geotail and ISEE 1/2 data [*Tsyganenko et al.,* 1998], we found that the twisting can be quite conspicuous even as close to Earth as $-20 \le X \le -10$, with a gra- dual increase of the twisting angle tailward. The numerical estimates of the twisting angle for different bins of the X coordinate make it possible to derive a quantitative relation between the twisting angle, the B_y component of the IMF, and tailward distance X. Here we will describe the method without giving a concrete model; for this reason we do not specify the dependence of the twisting

angle on X but merely assume that it is a known function of position in the tail.

For the sake of generality one can even introduce a dependence of the twisting angle on $\rho = (Y^2+Z^2)^{1/2}$. This allows one to model a more complex twisting of the current sheet, in which its cross section becomes S shaped. It is likely that such a deformation can develop in the tail, as was demonstrated by *Kaymaz et al.* [1995], *Tsyganenko et al.* [1998], and *White et al.* [1998] on the basis of data of IMP 8 and Geotail, and by MHD simulations, respectively.

4.1. Twist/Warp Transformation of the Tail Field

A natural way to introduce the twisting of the model tail current sheet, as well as its tilt-related warping in the Y–Z plane, is to represent the magnetic field in a cylindrical coordinate system (ρ, ϕ, X), coaxial with the tail axis, and to apply an appropriate deformation of the azimuthal coordinate ϕ, based on the above general equations (see also problem 14 in Appendix A of *Stern* [1994.]) More specifically, assuming that the general coordinates (f, g, h) in (5)–(6) are cylindrical coordinates (ρ, ϕ, X), coaxial with the Sun-Earth line, let us replace the azimuthal coordinate ϕ by a modified coordinate $F_0(\rho, \phi, X)$. From (5)–(6) one obtains the components of the distorted magnetic field as

$$\begin{aligned} B'_\rho &= B^*_\rho \frac{\partial F_0}{\partial \phi} \\ B'_\phi &= B^*_\phi - \rho\left[B^*_X \frac{\partial F_0}{\partial X} + B^*_\rho \frac{\partial F_0}{\partial \rho}\right] \\ B'_X &= B^*_X \frac{\partial F_0}{\partial \phi}, \end{aligned} \tag{13}$$

where the asterisks are used to denote "mapped" components, i.e., $B^*_{\rho,\phi,X} \equiv B_{\rho,\phi,X}(\rho, F_0, X)$.

One can see that taking $F_0(\rho, \phi, X)$ in the form

$$F_0 = \phi + G(X)\frac{\rho^3 \cos\phi}{\rho^4 + L^4(X)} \sin\Psi - \phi_t(\rho, X, B_y) \tag{14}$$

can provide the desired deformation of the current sheet. The second term on the right-hand side of (14) is responsible for the tilt-related warping of the sheet in the Y–Z plane and has a form equivalent to that assumed by *Tsyganenko* [1989, 1995, 1996], also used in the recent study of *Tsyganenko et al.* [1998]. That term is proportional to the sine of the geodipole tilt angle Ψ and includes an amplitude coefficient $G(X)$, whose magnitude gradually decreases with growing tailward distance. The scale distance $L(X)$ controls the spatial extent of the warping across the tail and can be assumed to be equal to the tail's radius at a given position on the tail axis.

Note that warping the current sheet by modifying the angle ϕ, as given by (13)–(14), introduces a tilt-related variation of the near-tail lobe field, consistent both with data and with the expected effect of the electric current redistribution. Indeed, for $\Psi > 0$ (northern summer conditions) the electric current flow lines in the near tail become convex/concave when viewed from the northern/southern lobe. As a result of the geometrical factor in the Biot-Savart formula, that effect should result in a larger magnetic field on the concave (southern) side of the current sheet (because of the symmetry, the effect reverses its sign for $\Psi < 0$). This is exactly what one formally obtains from the last equation in (13), taking into account that the derivative of the second term of (13) by ϕ is positive for $-\pi < \phi < 0$ (in the southern lobe) and negative for $0 < \phi < \pi$ (in the northern lobe). This effect should be more pronounced closer to Earth as a result of the growing contribution from the dipole, which increases the total B_x in the southern lobe but decreases it in the northern lobe (again, for $\Psi < 0$ the effect reverses its sign). In fact, this asymmetry of the dipole's contribution to the field in the lobes is partially responsible for the warping of the plasma sheet: the excessive magnetic pressure on one of its sides deforms the sheet and thereby restores the pressure balance.

To check the consistency with observations of the north-south asymmetry of the deformation (13)–(14), we compiled a set of tail lobe field data from the large set of magnetometer data of *Fairfield et al.* [1994]. The data were selected by imposing the following restrictions. First, data chosen for the study were only from relatively quiet periods ($0 \le K_p < 4-$), with the solar wind ram pressure within the interval $1 < P_d < 4$ nPa. The set was further reduced by selecting measurements made within near-tail lobes close to the midnight meridian and was divided into two subsets. The first subset had the data points in the range $-12 \le X_{GSM} < -10\,R_E$, $|Y_{GSM}| \le 4\,R_E$, and $6 < |Z_{GSM} - Z_S| < 12\,R_E$, where a simple formula $Z_S = 8\sin\Psi$ was used for estimating the position of the center of the current sheet as a function of the tilt angle. The second subset had data from a more distant region with $-14 \le X_{GSM} < -12\,R_E$, and in that case the intervals of Y and Z were slightly expanded: $|Y_{GSM}| \le 5\,R_E$, and $5 < |Z_{GSM} - Z_s| < 15\,R_E$. The numbers of data records in the two sets were 140 and 237, respectively. As we noted above, the tilt angle effect upon the southern lobe field should be opposite to that in the northern lobe. We nevertheless can combine the data taken in both lobes by converting southern lobe data points into "equivalent" northern ones, using the property of symmetry of the magnetosphere in the north-south direction [e.g., *Mead and Fairfield,* 1975]:

$$B(X, Y, -Z, \Psi) = B(X, Y, Z, -\Psi) \tag{15}$$

According to (15), the data from the southern lobe can be converted into the northern ones by changing the signs of both Z and Ψ.

Figure 4 shows the plots of the measured northern lobe field strength against the dipole tilt angle. A clear trend for stronger/weaker fields in the northern lobe for negative/positive tilt angles can be seen in both panels, in agreement with the asymmetry provided by the deformation (13)–(14). For the first interval, $-12 \le X_{GSM} < -10\,R_E$, a linear fit to the data points yields a variation of the northern lobe field between 32.4 and 58.8 nT as the geodipole tilt angle changes from $+35°$ to $-35°$. As expected, the tilt effect upon the lobe field becomes weaker at larger geocentric distances: for $-14 \le X_{GSM} < -12\,R_E$ the linear fit was found to vary within a narrower interval, between 32.4 and 43.2 nT, for the same range of Ψ.

To compare the above statistical result with the prediction of the model, the transformations (7) and (11)–(14)

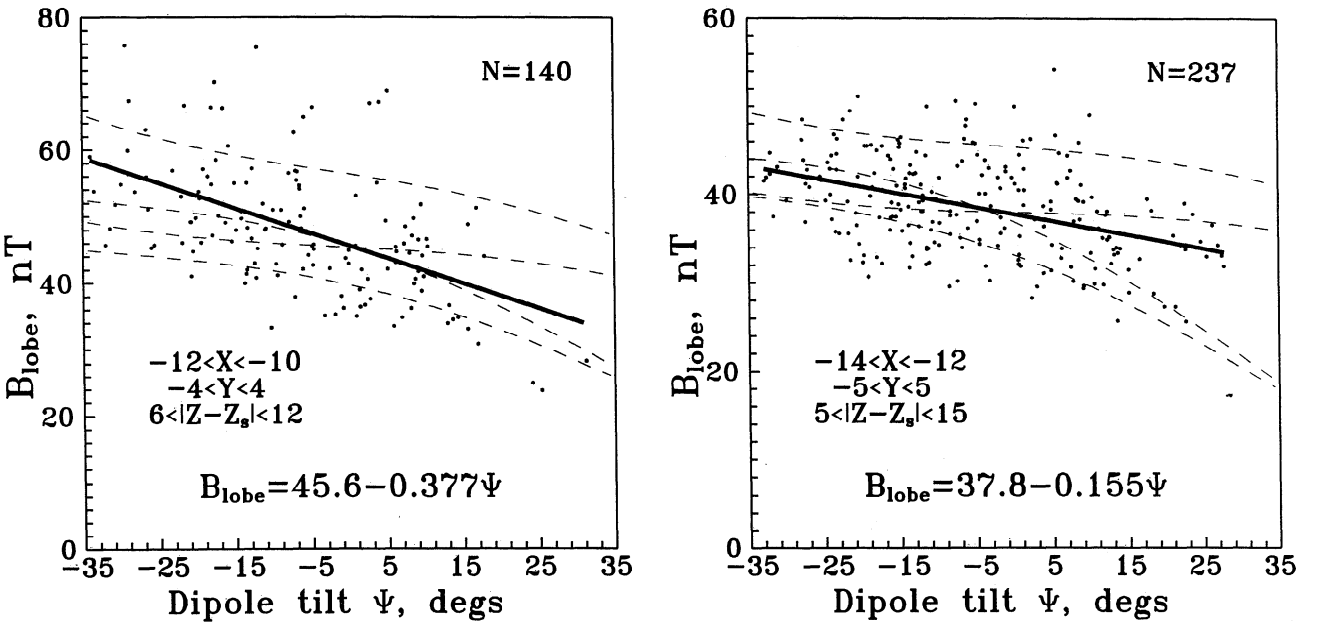

Figure 4. Observed strength of the total field in the northern lobe of the near magnetotail for two intervals of X_{GSM}, plotted against the Earth's dipole tilt angle. The measured values of B were taken from the magnetosphere modeling set of *Fairfield et al.* [1994]. Data from the southern lobe were also used with the opposite sign of the tilt angle, as explained in the text. Note a clear trend for a decrease of B as the dipole tilt varies from its minimal ($\sim -35°$) to maximal ($\sim +35°$) value. The four dashed lines in each panel indicate the tilt dependence of a model field calculated at four locations within the X–Z bins covered by the data.

were applied to the data-based model [*Tsyganenko*, 1996] with zero tilt, parameterized by average solar wind conditions with $P = 3$ nPa, $Dst = -10$ nT, IMF $B_y = 0$, and $B_z = -1$ nT. The parameters entering in the tilt transformation (7), (11)–(12) were specified as $R_{H0} = 8.3$, $R_{H1} = 0$, and $R_{H2} = -5.2$, while the warping parameters in (14) were set at $G = 50$ and $L = 20$, corresponding to the values found by *Tsyganenko et al.* [1998] for the nearest bin $-15 \le X_{GSM} < -10\,R_E$. Since the positions of the individual data points in Figure 4 are distributed within a relatively wide range of $\{X, Y, Z\}$, the tilt angle dependence of the model field was calculated at four positions in the midnight meridian plane (for each of two X_{GSM} bins in Figure 4), located close to the boundaries of the sampling regions. The corresponding variation of the model field with the tilt angle is shown in each panel of Figure 4 by dashed lines.

As can be seen from the plots, in both cases the observed and the model fields decrease as the tilt angle increases from negative to positive values. However, while at larger distances ($-14 \le X < -12$; right panel) the average slope of the model field is close to that of the data-based linear fit (thick solid line), in the nearest bin ($-12 \le X < -10$; left panel) the model effect is weaker than the observed one. An obvious explanation is that, because the geocentric distances are closer, the actual warping amplitude for the interval $-12 \le X < -10$ is significantly larger than that for $-14 \le X < -12$, while we assumed the same warping parameters in (14) for both cases. The observed relation between the tilt angle and the asymmetry of the near tail lobe field implies an interesting possibility to find the variation of the parameters of the warping function (14) along the tail, provided we have sufficiently dense coverage of the tail lobes by the data. This task extends beyond the scope of the present paper and is therefore relegated to future studies.

The last term in (14), ϕ_t, is the angle of the current sheet twisting with respect to the equatorial plane. It can be approximated by a simple analytical function, close to zero near Earth and gradually increasing with distance to some asymptotic value in the deep tail. The rate of the current sheet rotation and the asymptotic value of ϕ_t should depend on the values of the IMF B_y and B_z components. An appropriate model for ϕ_t can be devised, based either on data [*Tsyganenko et al.*, 1998] or on results of MHD si- mulations; that task was not pursued in the present work.

Note also that assuming $G = 0$ in (14) (i.e., ignoring the tilt-related effects) and substituting the resultant derivatives in (13), one can obtain after some algebra the Cartesian components of the twisted field as

$$\begin{aligned} B_x &= B_x^* \\ B_y &= B_y^* \cos\phi_t - B_z^* \sin\phi_t - Z\left(B_\rho^* \frac{\partial\phi_t}{\partial\rho} + B_x^* \frac{\partial\phi_t}{\partial X}\right) \\ B_z &= B_y^* \sin\phi_t + B_z^* \cos\phi_t + Y\left(B_\rho^* \frac{\partial\phi_t}{\partial\rho} + B_x^* \frac{\partial\phi_t}{\partial X}\right) \end{aligned} \qquad (16)$$

which are identical to those given by equation (8) of *Tsyganenko et al.* [1998], obtained in that paper by introducing an appropriate correction of the azimuthal component B_ϕ, which restored the condition $\nabla \cdot \mathbf{B} = 0$. Here we arrived at the same result by using the general deformation procedure. Figures 5 and 6 illustrate the effect of applying to the model of *Tsyganenko* [1996] the transformation (13)–(14)

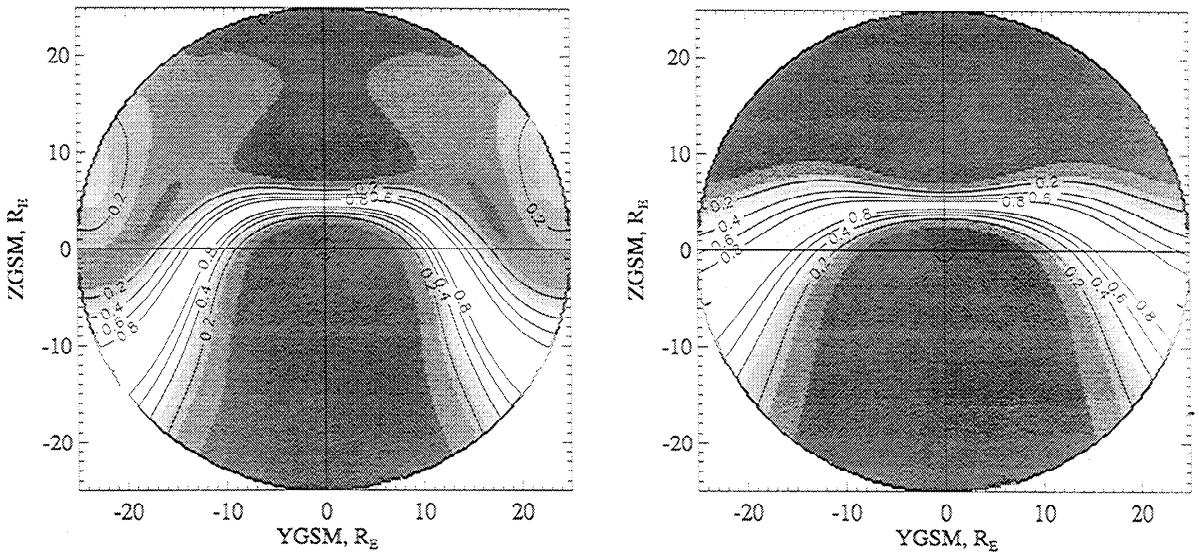

Figure 5. Illustration of the effect of warping of the model tail current sheet in the Y–Z plane, obtained by applying the deformation of the azimuthal angle $\phi = \tan^{-1}(Z/Y)$, as defined by (13)–(14). (left) A strong warping in the near tail at $-15 < X < -10\ R_E$; (right) a weaker warping in the middle tail at $-40 < X < -30\ R_E$. The tilt angle in both cases equals 35°. The brightness of the shading and the equal intensity lines correspond to the volume electric current density, normalized by its maximal values at the same Y_{GSM} positions.

without the twisting term ($\phi_t = 0$.) The plots in the two panels of Figure 5 show the distribution of the volume electric current density in the tail cross sections at two different locations, obtained for the maximal value of the dipole tilt angle $\Psi = 35°$. In the left plot the values of the warping parameters were $G = 50$ and $L = 20$, corresponding to the values obtained by *Tsyganenko et al.* [1998] from Geotail data for $-15 < X < -10\ R_E$, while the right panel shows the current sheet at larger distances, $-40 < X < -30\ R_E$, with $G = 35$ and $L = 25$. In both plots the brightness of the shading and the lines of equal intensity reflect the values of the electric current density j, normalized to its maximal value at a given Y_{GSM}. As a result of the adopted normalization the lines of equal intensity approximately correspond to the electric current flow lines.

Figure 6 shows in the same format the model electric current density for an untilted dipole, but with a nonzero twisting term. In the left panel a simple rotation of initially flat cur-

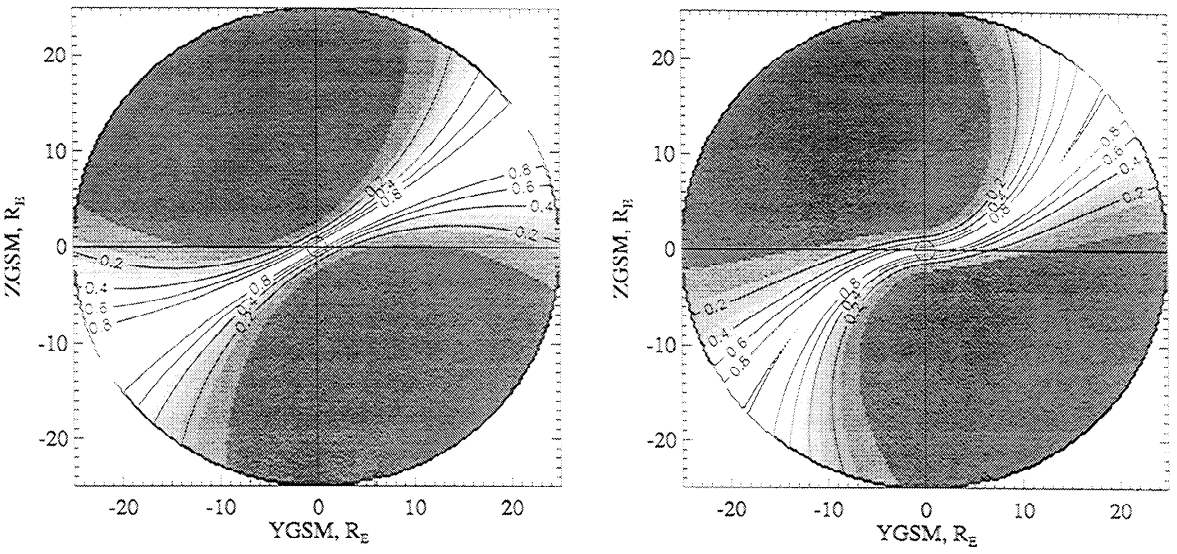

Figure 6. Illustration of the twisting effect of the IMF B_y, as replicated by the transformation (13)–(14) of the model field with $G = 0$. (left) A purely rotational deformation; (right) a differential rotation with the angle ϕ_t depending on ρ, which results in a distorted cross section of the current sheet. Note that the above distributions are not based on a specific data, but only demonstrate the flexibility of the mathematical model.

rent sheet by $\phi_t = 30°$ was applied, while in the right panel a dependence of ϕ_t on ρ was also introduced, resulting in a distortion of the sheet similar to that found by *Kaymaz et al.* [1995]. Note however, that the twisted electric current patterns shown in Figure 6 are not based on any specific data: the only purpose of these plots is to demonstrate the flexibility of the method in replicating possible IMF-induced deformations of the tail current sheet.

4.2. Using Deformations for Controlling the Thickness of the Cross-Tail Current Sheet

The deformed distribution of the tail field and current, obtained by using the transformation (13)–(14), can be further modified, adding more flexibility with regard to the variation of the current sheet thickness across the tail. In principle, the current sheet thickness can be controlled easily by an appropriate modification of the vector potential of the tail field [e.g., *Tsyganenko and Peredo,* 1994]. In this respect one might wonder why was it necessary to devise another deformation instead of using the seemingly simpler way. The answer, again, is that any recalibration of the existing cross-tail field terms would require a lengthy and cumbersome recalculation of the corresponding shielding fields. In contrast, the method of deformations allows one to easily modify the electric current distribution and, at the same time, keeps the total field fully confined within the magnetopause.

To modify the rate of the current sheet flaring toward its flanks, it suffices to locally change the rate of the variation with ϕ of the "mapped" azimuthal angle F_0 in (13)–(14), so that it would decrease in the vicinity of the current sheet and slightly increase in the tail lobes. Also, the distortion magnitude should gradually decrease toward the tail's center, so that the field and current in the middle of the tail would remain unchanged. These conditions can be met with the following transformation of the angle F_0:

$$F = F_0 - u\frac{\rho^2}{\rho^2 + R_T^2}\sin 2F_0$$

where the parameter u controls the degree of additional flaring of the current sheet over the scale distance R_T of the order of the tail's radius. However, as a close inspection of the resultant electric current distributions revealed, the purely sinusoidal deformation of the azimuthal angle provided insufficient modification of the current sheet. At the same time it gave rise to broadly distributed unphysical currents, extending deep into the tail lobes. Much better results were obtained with a slightly more complicated function with an additional parameter v,

$$F = F_0 - u\frac{\rho^2}{\rho^2 + R_T^2}\sin(2F_0 + v\sin 2F_0) \qquad (17)$$

where $0 < v < 1$. Positive values of the parameter u result in a slower variation of F in the vicinity of $F_0 = 0$ and $F_0 = \pi$, providing a broadening of the current sheet, while for negative u the effect reverses, resulting in a thinner sheet. Figure 7 illustrates how the modification (17) of the angle F affects the geometry of the tail current: it yields a more rapid expansion of the sheet toward the flanks for $u > 0$ and an opposite effect for $u < 0$.

5. Summary and Concluding Remarks

In this paper we have demonstrated several uses of the deformation method in modeling the large-scale magnetospheric configuration. The method offers a simple way to replicate the distortion of the magnetospheric magnetic field and of the associated electric current due to seasonal and diurnal wobbling of the Earth's dipole, as well as the twisting of the tail current sheet caused by the azimuthal component

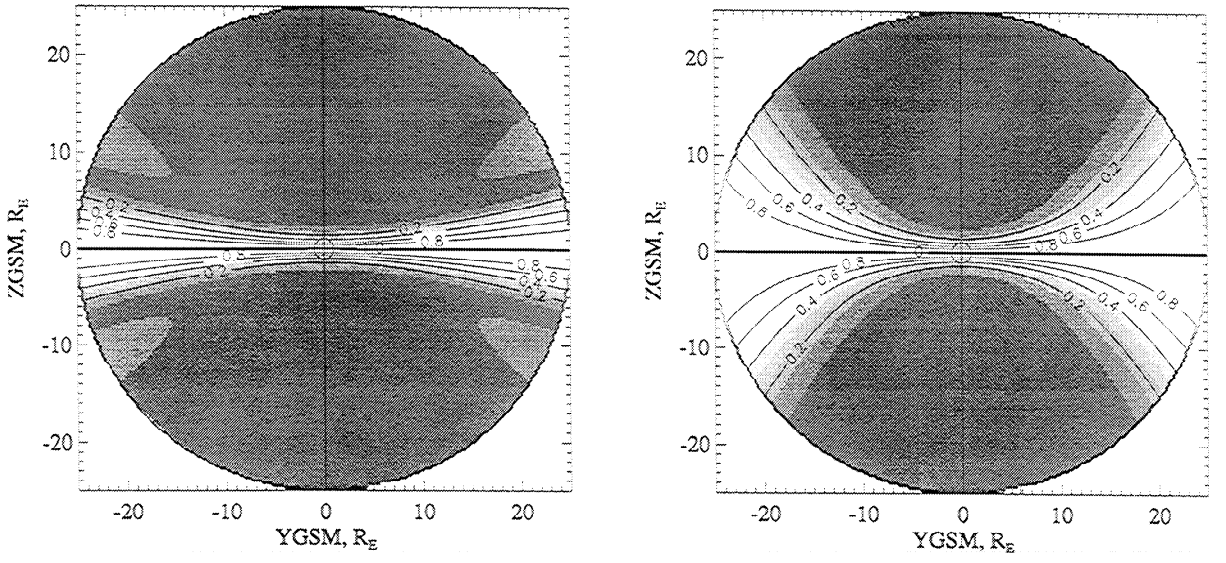

Figure 7. Illustration of the effect of the transformation (16) of the angle ϕ, allowing one to change the rate of the current sheet expansion toward the tail flanks. (left) $u = -0.25$ and $v = 0.8$ result in a slower expansion of the sheet; (right) $u = 0.08$ with the same $v = 0.8$ yield a much thicker current sheet near the tail's flanks.

of the IMF. An interesting side effect of the tail "bending" transformation is the concurrent deformation of the magnetopause: despite its being a purely geometrical corollary of the radially dependent rotation (7) it replicates the actually observed tilt-related motion of the magnetopause and, by an appropriate modification of parameters, can be brought into quantitative agreement with data. Various kinds of deformations can be superposed on one another, offering a remarkable flexibility and allowing one to model realistic magnetospheric configurations without violating the condition $\nabla \cdot \mathbf{B} = \mathbf{0}$. Since we no longer need to separately introduce the tilt effects in the shielding fields for each source of the external field, using a single deformation allows one to drastically simplify the model codes and hence accelerate its performance. The deformation method offers an effective way of keeping under control the normal component of the magnetic field on the magnetopause, regardless of the distortions of magnetospheric currents caused by the dipole tilt and by the IMF.

It is worth noting here another effect of the IMF upon the tail that can also be treated by imposing a simple deformation. This is the flattening of the tail cross section due to the anisotropy of the external magnetic pressure, first predicted by *Michel and Dessler* [1970]. The effect was extensively discussed by *Sibeck et al.* [1986b] and confirmed by both MHD models and deep-tail data of Geotail [e.g., *Frank et al.*, 1995]. A straightforward way of replicating the flattening is to scale the Cartesian coordinates Y' and Z', orthogonal to the tail axis and rotated by the IMF clock angle around that axis. The magnitude of the scaling factors for both axes should be made a slowly growing function of the tailward distance, so that the flattening would gradually increase down the tail. A more detailed treatment of this effect extends beyond the scope of the present work and hence is not further pursued.

With regard to deficiencies of the method, two basic facts should be pointed out. The first one is the inability of the deformation technique to change the topology of the field lines. In the case of the bending deformation of the total magnetospheric field, discussed in section 3, that resulted in a lack of dependence of the polar cusp latitude upon the dipole tilt angle. A compromise solution to that problem has been outlined in the Appendix, in which we abandon the deformation of the Earth's internal field and treat it separately in a more standard way; i.e., we combine the tilted dipole field with an extended tilt-dependent expansion for the shielding field, taking into account the tilt-related deformation of the magnetopause.

Another limitation of the method is related to the need of keeping under control the artificial electric currents induced by the deformations. This imposes some restrictions on the choice of coordinate transformation and makes it necessary to check final distributions of the electric current density. In most cases, only smooth and gradual distortions of coordinates are acceptable.

Besides the terrestrial magnetosphere modeling, the deformation method can be successfully used in representing the magnetic fields of other planets. In particular, the twisting/warping effect is quite pronounced in the Jovian magnetosphere, because of the fast rotation of the planet. *Khurana* [1997] successfully used Euler potentials for modeling the resulting complex shape of the Jovian current disk. As we noted above, the described approach does not need any knowledge of Euler potentials. Combined with the variety of existing methods for modeling magnetic fields of disk-like current sheets, it can boost further progress in modeling planetary magnetospheres.

Appendix: Shielding of the Dipole Field Within a Boundary With Tilt-Dependent Shape

We are using here the least squares shielding approach [*Schulz and McNab*, 1987; *Tsyganenko*, 1995] for confining the dipole field within a magnetopause with a predetermined shape. However, in previous models [e.g., *Tsyganenko*, 1989, 1995, 1996] derivation of the shielding field for the dipole was greatly simplified as a result of two assumptions. First, the axial symmetry of the boundary, combined with a simple dependence of the normal component of the dipole field on the azimuthal angle, allowed us to reduce the dimensionality of expansions for the scalar potential of the shielding field, retaining only two coordinates instead of three. Second, the assumed independence of the boundary shape on the tilt angle Ψ made it possible to represent the solution for an arbitrary Ψ as a linear combination of the shielding fields for $\Psi = 0$ and $\Psi = \pi/2$.

In the present formulation, both assumptions are no longer valid: for $\Psi \neq 0$ the magnetopause becomes axially asymmetric, and the degree of that asymmmetry changes with the tilt angle. However, as we show below, a relatively simple extension of the previously used method still allows us to obtain an accurate solution.

Initially, we tried to extend the original expansions in cylindrical harmonics by adding more degrees of freedom with respect to the azimuthal angle, a step made necessary by the breakdown of the axial symmetry. However, much better results were obtained by replacing cylindrical harmonics with the cartesian "box" potentials, used by *Tsyganenko* [1995] for representing the shielding field for the cross-tail current sheet,

$$U_1 = \sum_{i=1}^{N}\sum_{k=1}^{N}(a_{ik} + b_{ik}\cos\Psi)\exp\left[\left(\frac{1}{p_i^2} + \frac{1}{r_k^2}\right)X\right] \times \cos\frac{Y}{p_i}\sin\frac{Z}{r_k} \tag{A1}$$

$$U_2 = \sum_{i=1}^{N}\sum_{k=1}^{N}(c_{ik}\sin\Psi + d_{ik}\sin 3\Psi)\exp\left[\left(\frac{1}{q_i^2} + \frac{1}{s_k^2}\right)X\right] \times \cos\frac{Y}{q_i}\cos\frac{Z}{s_k} \tag{A2}$$

The potentials (A1) and (A2) correspond to two types of symmetry of the field with respect to the Z coordinate. Their coefficients a_{ik}, b_{ik}, c_{ik}, d_{ik} and the scale length parameters p_i, r_k, q_i, s_k were fitted by least squares to minimize the rms residual $\langle B_n^2 \rangle$ over a set of 2232 points, evenly distributed both in geometrical space (i.e., on the boundary, up to $X \sim -80\,R_E$ down the tail) and in the space of the tilt angle $-35° \leq \Psi \leq 35°$. The shape of the model magnetopause for

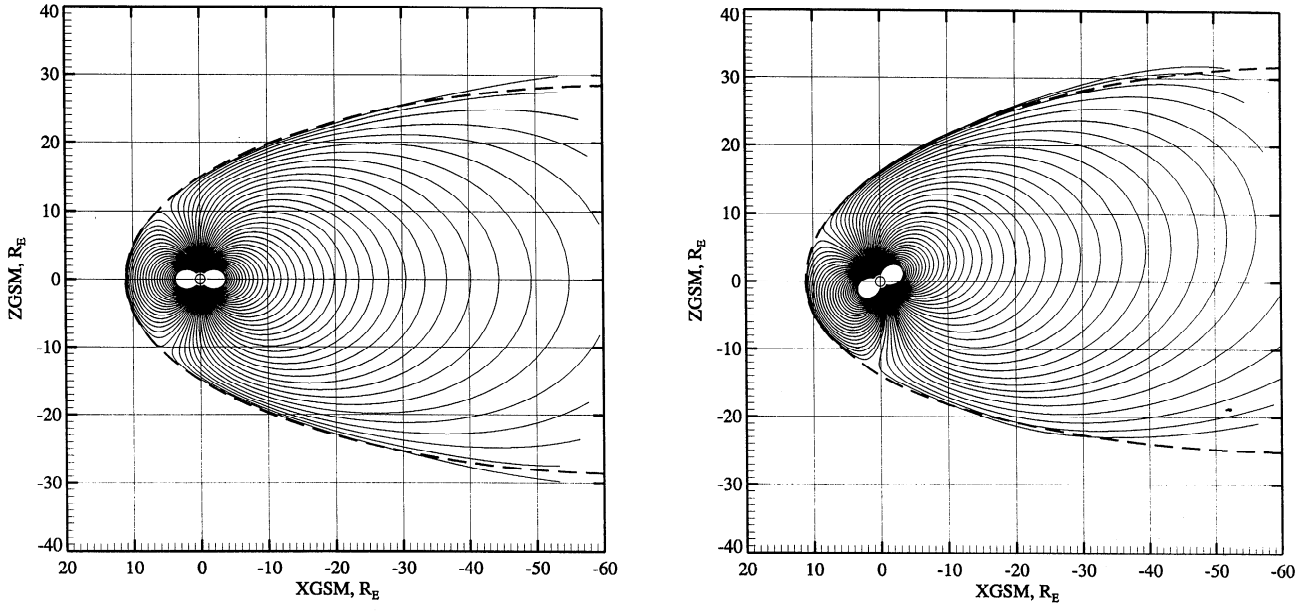

Figure 8. Lines of the dipolar magnetic field, shielded within the tilt-dependent magnetopause. (left) Untilted configuration ($\Psi = 0$); (right) a tilted dipole with $\Psi = 30°$.

$\Psi = 0$ was chosen identical to that used in the existing version of the magnetospheric field model [*Tsyganenko,* 1995, 1996], that is, an axially symmetric hemi-ellipsoid in the cislunar region, smoothly continued by a cylinder tailward from $X \approx 65\ R_E$. For nonzero tilt angles, both the positions of the boundary points and corresponding unit normals are affected by the deformation and hence were recalculated from (7)–(12).

We also found that a significant increase in the accuracy of the shielding is achieved with the same number of terms in the expansion, by introducing a rotation of the potential fields (A1) and (A2). More specifically, instead of the sum of shielding fields $\mathbf{B_1}(\mathbf{r}) = -\nabla U_1$ and $\mathbf{B_2}(\mathbf{r}) = -\nabla U_2$, corresponding to the potentials (A1) and (A2), we used

$$\mathbf{B} = \hat{\mathbf{R}}_1^{-1}\mathbf{B}_1(\hat{\mathbf{R}}_1\mathbf{r}) + \hat{\mathbf{R}}_2^{-1}\mathbf{B}_2(\hat{\mathbf{R}}_2\mathbf{r}) \qquad \text{(A3)}$$

where $\hat{\mathbf{R}}_1 = \hat{\mathbf{R}}_1(\gamma_1)$ and $\hat{\mathbf{R}}_2 = \hat{\mathbf{R}}_2(\gamma_2)$ are the matrices of rotation around the Y_{GSM} axis. The angles of the rotation, γ_1 and γ_2, were assumed to be proportional to the dipole tilt angle: $\gamma_1 = \kappa_1\Psi$ and $\gamma_2 = \kappa_2\Psi$, where the coefficients κ_1 and κ_2 were determined by least squares together with other free parameters. For $\Psi = 0$ the shape of the model magnetopause was defined similarly to that in the existing magnetospheric model [*Tsyganenko,* 1995, 1996], i.e., as an axially symmetrical hemi-ellipsoid, continued by a cylinder in the far tail. In the case $\Psi \neq 0$ the tilt-induced distortion of the magnetopause was taken into account, using the transformation (7)–(12) for calculating shifted positions of the boundary points and modified unit normal vectors.

Fitting the above expansions (A1)–(A3) with $N = 3$ resulted in the overall rms resudual normal field of 0.4% of the maximal B_n for the unshielded dipole field. That particular version of the shielding field model contained in total 18 coefficients and 14 nonlinear parameters. Figure 8 shows the lines of the shielded dipole field for two values of the tilt angle.

Acknowledgments. The author acknowledges David Sibeck for making available his set of the magnetopause crossings. Special thanks are due to David Stern for his careful reading of the manuscript, many valuable comments, and useful suggestions. This work is supported by NASA grants NAS5-32350 and NASW-97024 (ISTP GI Program) and by NSF Magnetospheric Physics Program grant ATM-9501463.

The Editor thanks Xiaoyan Zhou and Richard L. Kaufmann for their assistance in evaluating this paper.

References

Cowley, S. W. H., Magnetospheric asymmetries associated with the Y-component of the IMF, *Planet Space Sci., 29,* 79, 1981.

Eastman, T. E., S. A. Boardsen, and S. F. Fung, Configuration of high-latitude boundaries as observed by the Hawkeye satellite, *Eos Trans. AGU, 78*(46), Fall Meet. Suppl., F596, 1997.

Fairfield, D. H., A statistical determination of the shape and position of the geomagnetic neutral sheet, *J. Geophys. Res., 85,* 775–780, 1980.

Fairfield, D. H., N. A. Tsyganenko, A. V. Usmanov, and M. V. Malkov, A large magnetosphere magnetic field database, *J. Geophys. Res., 99,* 11,319-11,326, 1994.

Frank, L. A., et al., Observations of plasmas and magnetic fields in Earth's distant magnetotail: Comparison with a global MHD model, *J. Geophys. Res., 100,* 19,177–19,190, 1995.

Kaymaz, Z., G. L. Siscoe, J. G. Luhmann, J. A. Fedder, and J. G. Lyon, Interplanetary magnetic field control of magnetotail field: IMP 8 data and MHD model compared, *J. Geophys. Res., 100,* 17,163–17,172, 1995.

Khurana, K., Euler potential models of Jupiter's magnetospheric field, *J. Geophys. Res., 102,* 11,295–11,306, 1997.

Mead, G. D., and D. H. Fairfield, A quantitative magnetospheric model derived from spacecraft magnetometer data, *J. Geophys. Res., 80,* 523–534, 1975.

Michel, F. C., and A. J. Dessler, Diffusive entry of solar flare

particles into the geomagnetic tail, *J. Geophys. Res., 75,* 6061–6072, 1970.

Murayama, T., Spatial distribution of energetic electrons in the geomagnetic tail, *J. Geophys. Res., 71,* 5547–5557, 1966.

Newell, P. T., and C.-I. Meng, Dipole tilt effects on the latitude of the cusp and cleft/low-latitude boundary layer, *J. Geophys. Res., 94,* 6949–6954, 1989.

Russell, C. T., The configuration of the magnetosphere, in *Critical Problems of Magnetospheric Physics,* edited by E. R. Dyer, pp.1–16, IUCSTP Sec., Nat. Acad. of Sci., Washington, D. C., 1972.

Russell, C. T., and K. I. Brody, Some remarks on the position and shape of the neutral sheet, *J. Geophys. Res., 72,* 6104–6106, 1967.

Schulz, M., and M. McNab, Source-surface model of the magnetosphere, *Geophys. Res. Lett., 14,* 182–185, 1987.

Sibeck, D. G., G. L. Siscoe, J. A. Slavin, E. J. Smith, B. T. Tsurutani, and R. P. Lepping, The distant magnetotatil's response to a strong interplanetary magnetic field B_y: Twisting, flattening, and field line bending, *J. Geophys. Res., 90,* 4011–4019, 1985.

Sibeck, D. G., J. A. Slavin, E. J. Smith, and B. T. Tsurutani, Twisting of the geomagnetic tail, in *Solar Wind–Magnetosphere Coupling,* edited by Y. Kamide and J. A. Slavin, pp. 731–738, Terra Sci., Tokyo, 1986a.

Sibeck, D. G., G. L. Siscoe, J. A. Slavin, and R. P. Lepping, Major flattening of the distant geomagnetic tail, *J. Geophys. Res., 91,* 4223–4237, 1986b.

Sibeck, D. G., R. E. Lopez, and E. C. Roelof, Solar wind control of the magnetopause shape, location, and motion, *J. Geophys. Res., 96,* 5489–5495, 1991.

Stern, D. P., Parabolic harmonics in magnetospheric modeling: The main dipole and the ring current, *J. Geophys. Res., 90,* 10,851–10,863, 1985.

Stern, D. P., Tail modeling in a stretched magnetosphere, 1, Methods and transformations, *J. Geophys. Res., 92,* 4437–4448, 1987.

Stern, D. P., The art of mapping the magnetosphere, *J. Geophys. Res., 99,* 17,169–17,198, 1994.

Tsyganenko, N. A., A magnetospheric magnetic field model with a warped tail current sheet, *Planet. Space Sci., 37,* 5–20, 1989.

Tsyganenko, N. A., Quantitative models of the magnetospheric magnetic field: Methods and results, *Space Sci. Rev., 54,* 75–186, 1990.

Tsyganenko, N. A., Modeling the Earth's magnetospheric magnetic field confined within a realistic magnetopause, *J. Geophys. Res., 100,* 5599–5612, 1995.

Tsyganenko, N. A., Effects of the solar wind conditions on the global magnetospheric configuration as deduced from data-based field models, *Eur. Space Agency Spec. Publ., ESA SP-389,* 181–185, 1996.

Tsyganenko, N. A., An empirical model of the substorm current wedge, *J. Geophys. Res., 102,* 19,935–19,941, 1997.

Tsyganenko, N. A., and M. Peredo, Analytical models of the magnetic field of disk-shaped current sheets, *J. Geophys. Res., 99,* 199–206, 1994.

Tsyganenko, N. A., and D. P. Stern, Modeling the global magnetic field of the large-scale Birkeland current systems, *J. Geophys. Res., 101,* 27,187–27,198, 1996.

Tsyganenko, N. A., S. B. P. Karlsson, S. Kokubun, T. Yamamoto, A. J. Lazarus, K. W. Ogilvie, and C. T. Russell, Global configuration of the magnetotail current sheet as derived from Geotail, Wind, IMP 8, and ISEE 1/2 data, *J. Geophys. Res., 103,* 6827–6842, 1998.

Voigt, G.-H., A mathematical magnetospheric model with independent physical parameters, *Planet. Space Sci., 29,* 1–20, 1981.

White, W. W., G. L. Siscoe, G. M. Erickson, Z. Kaymaz, N. C. Maynard, K. D. Siebert, B. U. O. Sonnerup, and D. R. Weimer, The magnetospheric sash and the cross-tail S, *Geophys. Res. Lett., 25,* 1605–1608, 1998.

N. A. Tsyganenko, Raytheon STX Corporation, Laboratory for Extraterrestrial Physics, Code 690.2, NASA Goddard Space Flight Center, Greenbelt, MD 20771. (e-mail: kolya@nssdca.gsfc.nasa.gov)

(Received January 30, 1998; revised June 17, 1998; accepted June 26, 1998.)